Design of Diffusive Modified Chessboard Metasurface

Mustafa K. Taher Al-Nuaimi [ID], Wei Hong [ID], *Fellow, IEEE*, and Yejun He [ID], *Senior Member, IEEE*

Abstract—In this letter, the design of ultrathin diffusive modified chessboard metasurface at microwave band is presented. Each quadrant of the conventional 2×2 chessboard is replaced by a small size 1-bit reflectarray exhibiting an optimized diffusive 1-bit quantized phase distribution. Furthermore, the proposed chessboard metasurface is designed in such a way to also have 180° phase shift between any adjacent quadrants (reflectarrays). A subwavelength-spaced cross-polarization rotating anisotropic unit cell, which can rotate the polarization of a linearly polarized incident wave to its orthogonal (cross polarized) component with 99% polarization conversion efficiency from 7 to 16 GHz, is used to compose a two small size 1-bit reflectarrays. The proposed unit cell and its mirror image are used to provide the required 1-bit phase states ("0°" and "180°") of the 8×8 unit cells reflectarrays. The proposed diffusive metasurface is composed of four reflectarrays and has an aperture dimensions of $160 \times 160 \times 3.04$ mm³. Both simulation and measurement results show that the proposed metasurface can diffuse the incident electromagnetic wave regardless of the polarization of the incident wave and under wide angle of incidence (up to 60°) with 10 dB radar cross reduction when compared to a PEC plate of same size.

Index Terms—Diffuse scattering, metasurface, reflectarray.

I. INTRODUCTION

METASURFACE has attracted a lot of attention among science and engineering researchers due to their strong capabilities in controlling (manipulating) the characteristics of electromagnetic (EM) waves [1]–[10]. The metasurface for RCS reduction can be designed as passive, active, digital or programmable metasurface [11], [12]. In [13]–[16], chessboard and checkerboard metasurfaces with about 180° ± 37° reflection phase difference between any adjacent quadrants on its aperture were proposed for RCS reduction. The unit cells in each quadrant have the same orientation, phase, and dimensions. However, the scattering patterns of such surfaces contain intense diffraction lobes in the diagonal planes [17]. The bandwidth of chessboard surface was improved using various techniques [18], [19]; however, the scattering patterns still have intense diffraction lobes in the diagonal planes.

The using of focusing reflection phase or reflectarray for EM-wave diffusion (and RCS reduction) have been a hot topic recently and various designs have been proposed in the literature such as multibeam reflectarray technique by redirecting the backscattered energy away from the boresight axis in [20], using tapered graded dielectric perforation and focusing reflection phase in [21], the metasurface of unit cells have concave and convex parabolic phase distributions in [4]. For a circularly polarized incident wave, an approach in [3] was proposed for backscattered EM-wave diffusion using Pancharatnam–Berry unit cell to compose a number of small size subarrays exhibiting focusing parabolic reflection phase, and the small size subarrays are distributed according to a 1-bit and 2-bit codes.

In this letter, an ultrathin and polarization-independent diffusive modified chessboard like metasurface for low-level diffusion of EM-waves under wide angle of incidence is developed. Each quadrant of the four quadrants of the conventional 2×2 chessboard metasurface is occupied by a 1-bit reflectarray exhibiting 1-bit quantized parabolic reflection phase. A cross-polarization conversion principle is used to design the 1-bit reflectarrays using anisotropic unit cell has four plasmonic resonances with more than 99% of cross polarization rotation efficiency. The anisotropic unit cell and its mirrored image are used together to realize the diffusive 1-bit quantized phase states (0°/180°) of the reflectarrays.

II. DESIGN OF POLARIZATION ROTATING UNIT CELL

The configuration of the proposed anisotropic unit cell (Bit 0 and Bit 1) is shown in Fig. 1(a). It consists of a copper resonator printed on the upper side of a grounded dielectric material ($\varepsilon_r = 3.38$, thickness $= 3.04$ mm $= 0.1\lambda_{10\text{GHz}}$) with a period $P = 10$ mm ($0.33\lambda_{10\text{GHz}}$). The reflection characteristics of the proposed anisotropic unit cell are numerically investigated using CST Microwave Studio and the optimized structural parameters are shown in Fig. 1. An intuitive scheme of the incident and reflected field vectors of the proposed anisotropic unit cell are shown in Fig. 1(b). The incident electric field (E_i) would decompose into two orthogonal components (E_{iu} and E_{iv}). The subscripts "r" and "i" indicate the reflected and incident components, respectively. Because of its anisotropy, the unit cell (Bit 0) and its mirror image (Bit 1) rotate the polarization of the incident wave (by 90°) to y-axis and $-y$-axis, respectively. Fig. 2(a) and (b) shows the magnitude and phase of the reflected components E_{ru} and E_{rv}, respectively. Both components have strong reflection with their reflection phases are continuous and
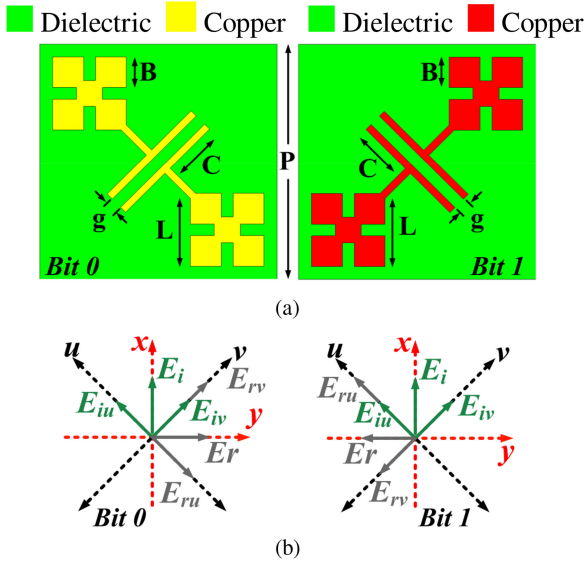
Fig. 1. (a) Front side of the proposed anisotropic unit cell: $P = 10$, $B = 1.3$, $C = 2.35$, $L = 3.1$, $g = 0.2$ all in mm. (b) Incident and reflected field vectors of the unit cell (Bit 0) and its mirrored unit cell (Bit 1).
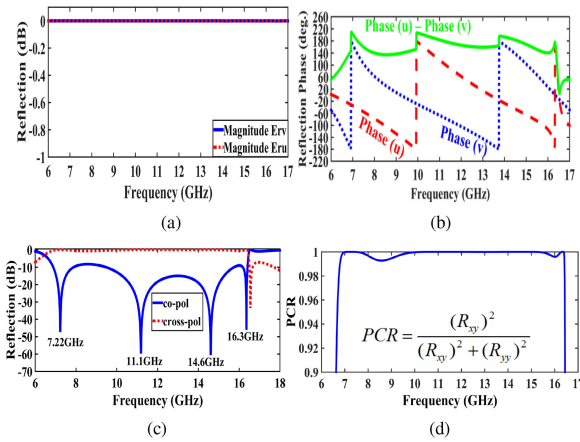

Fig. 2. (a) Magnitude and (b) phase of Eru and Erv. (c) Copol and cross-pol reflection coefficients. (d) PCR.

vary between $\pm 180°$ and the phase difference between those two components is within the range $180° \pm 30°$. The copolarization (copol) and cross-polarization (cross-pol) reflection coefficients of the proposed unit cell are shown in Fig. 2(c) and a very strong cross-pol conversion is achieved from 6.8 to 16.2 GHz and the polarization of the incident EM-wave will be rotated by 90° and reflected back. The unit cell has four plasmon resonances at 7.22 and 16.3 GHz (magnetic resonance), 11.1 and 14.6 GHz (electric resonance). As the copol reflection is < -10 dB over the frequency band of interest, it is, therefore, predicted that the efficiency of the polarization conversion would be high. Polarization conversion ratio (PCR) can be expressed using the formula in Fig. 2(d) where R_{xy} = cross-pol reflection and R_{yy} = copol reflection. The proposed unit cell can rotate the polarization of the incident wave with PCR $> 99\%$ from 7 to 16.2 GHz, which means that more than 99% of the incident wave is rotated into its cross-pol component and reflected back in this frequency band.

III. DIFFUSIVE METASURFACE DESIGN

As shown in [13]–[16], there is an 180° phase shift between the adjacent quadrants of a conventional chessboard metasurface and the unit cells in each quadrant have the same phase shift and same orientation. The proposed design also has an 180° phase shift between its four adjacent quadrants (reflectarrays) but the unit cells inside each quadrant are distributed according to a diffusive 1-bit parabolic reflection phase. The design procedure of the proposed chessboard metasurface was started by designing an 8×8 reflectarray with a 360° reflection phase range. A ray tracing principle is applied to find the required phase compensation at each unit cell the of 8×8 reflectarray with the aid

$$\phi\left(x_{ij}, y_{ij}\right) = \frac{2\pi}{\lambda}\left[\sqrt{x_{ij}^2 + y_{ij}^2 + F^2} - F\right] + \psi \pm 2n\pi. \quad (1)$$

In (1), the term $(2\pi/\lambda)$ is the propagation constant in vacuum with λ is the free space wavelength, x_{ij} and y_{ij} are the coordinates of the ijth unit cell in xy-plane, ψ is a phase constant, the term $2n\pi$ is added to keep the phase within 360° range. In (1), F is the distance from the focal point to the ijth unit cell. F is optimized carefully such that the reflectarray in each quadrant will diffuse the far-field incident EM-wave. In the optimization process of F, the reflectarray is considered as M $\times$ N array of unit cells and a MATLAB script based on the formulas in [12], [22], and [23] are used to find the optimum value of F and the phase distribution of the reflectarray. The phase distribution of a two 8×8 reflectarrays with maximum phase range of 360° is shown in Fig. 3(a) and (b) for $\psi = 0°$ and 180°, respectively. Using two different values of ψ will ensure the required phase shift between the adjacent quadrants of the proposed chessboard metasurface. In 1-bit phase quantization, only two types of unit cells with discrete phases of 0° and 180° are required to realize the 1-bit reflectarray and transmitarray [24]–[26]. In 1-bit phase quantization, the value of the reflection phase $\Phi_{1\text{-bit}} = 0°$ (bit 0) if $0° < \phi(x_{ij}, y_{ij}) < 180°$, otherwise $\Phi_{1\text{-bit}} = 180°$ (bit 1) [24], [25]. The optimized 1-bit phase distribution of the two reflectarrays is shown in Fig. 3(c) and (d). The 1-bit phase states are obtained by rotating the unit cell by 90° and without changing its structural parameters. The layout of the designed 1-bit reflectarrays are shown in Fig. 3(e) and (f) for $\psi = 0°$ and 180°, respectively. Layouts and phase distribution map of a three surfaces are shown in Fig. 4, which includes cross polarization converter metasurface (surface#1), a conventional 2 $\times$ 2 chessboard (surface#2), and the proposed 1-bit reflectarray modified chessboard (surface#3). Fig. 5 shows patterns of the two-dimensional (2-D) field scattering of the three surfaces. According to the 2-D field distribution, the cross polarization converter metasurface is strongly reflecting the incident EM-wave with 90° polarization rotation and without any change in the pattern shape as shown in Fig. 5(a). On the other hand, the conventional chessboard pattern shows four symmetric grating lobes in the diagonal planes [13]–[16]. For the proposed modified chessboard metasurface, a diffuse scattering is dominated and scattering level is much lower compared to surface#1 and surface#2 as shown in Fig. 5(c). The 3-D scattering patterns of the three surfaces and a PEC plate of same size under normal incidence of linearly polarized (LP) wave are shown in Fig. 6.
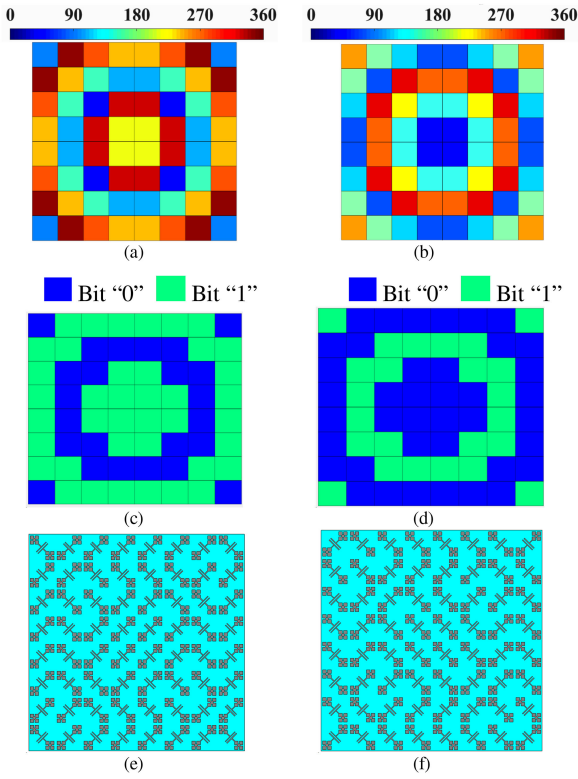
(a)

(b)

(c)

Fig. 3. Phase distribution of the 8×8 reflectarray for 360° phase range when $F = 5$ mm and the term ψ in (1) is: (a) $\psi = 0°$ and (b) $\psi = 180°$. Layout of the 1-bit phase quantization reflectarray when (c) $\psi = 0°$ and (d) $\psi = 180°$. Realization of the 1-bit reflectarrays using the polarization rotating unit cell when $F = 5$ mm and (e) $\psi = 0°$ and (f) $\psi = 180°$.
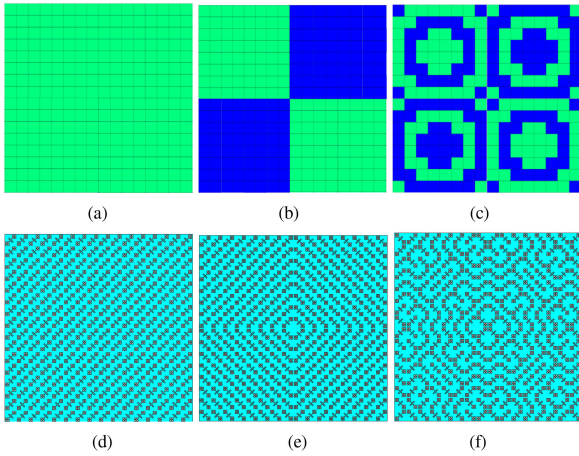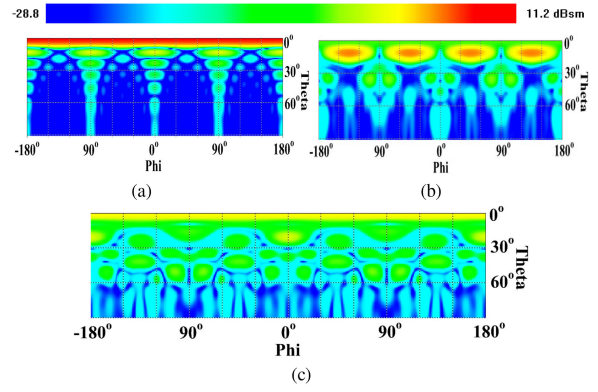
Fig. 5. 2-D far-field scattering patterns of (a) Surface#1, (b) Surface#2, and (c) Surface#3.
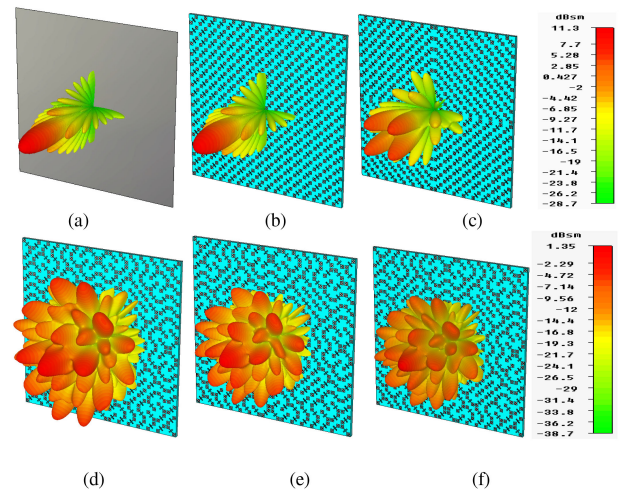

Fig. 6. 3-D scattering patterns when illuminated by LP wave of (a) PEC plate, (b) Surface#1, (c) Surface#2, and (d) Surface#3. The 3-D scattering patterns of the Surface#3 when illuminated by (e) LHCP and (f) RHCP circularly polarized wave.

Fig. 4. Unit cell distribution of (a) cross-polarization converter metasurface (surface#1) and (b) conventional 2×2 chessboard (surface#2) and (c) the proposed reflectarray chessboard (surface#3). Layouts of the three designed surfaces are in (d)–(f), respectively.

In the case of a PEC plate and surface#1, a very strong reflection in +z-direction is dominated as stated by Snell's law of reflection as shown in Fig. 6(a) and (b). According to the antenna array theory, Surface#2 redirects the backscattered energy as four symmetrical lobes along the diagonals as shown in Fig. 6(c) [13]–[16]. However, as shown in Fig. 6(d), the proposed structure (surface#3) redirects the backscattered energy

into a countless number of low-level lobes in a form of diffuse reflection as a result of the optimized diffusive phase distribution of the reflectarrays. The 3-D scattering patterns of surface#3 when it is illuminated by LHCP and RHCP circularly polarized wave are shown in Fig. 6(e) and (f), respectively. In both cases a low-level diffused scattering is dominated. The scattering characteristics of surface#3 under oblique illumination are investigated as shown in Fig. 7 and the scattering patterns of a bare PEC plate are also presented for comparison. As can be seen when the incident angle is increased to 45° and 60°, surface#3 still have low-level diffusion scattering, which is 10 dB less than that of a PEC plate that is scattered the EM-wave according to Snell's law of reflection [27], [28]. Furthermore, surface#3 can also efficiently diffuse the backscattered EM-wave regardless of the polarization of the incident EM-wave as shown in Fig. 8 when ($\theta_{inc} = 30°$, $\varphi_{inc} = 30°$), ($\theta_{inc} = 45°$, $\varphi_{inc} = 45°$), and ($\theta_{inc} = 60°$, $\varphi_{inc} = 60°$). As can be seen, for a PEC plate, the specular reflection is dominated while the diffused reflection is dominated for the proposed surface. The results show that the proposed metasurface has excellent scattering characteristics for
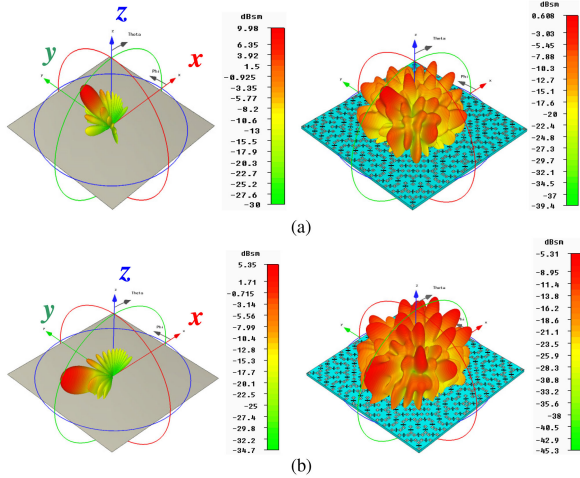
Fig. 7. 3-D scattering patterns of the proposed reflectarray chessboard and a PEC plate of same size under oblique incident when: (a) $\theta_{inc} = 45°$ and (b) $\theta_{inc} = 60°$.
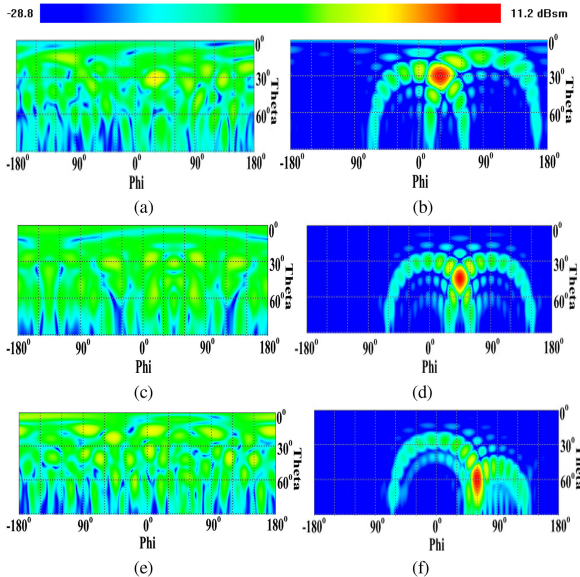

Fig. 8. 2-D far-field scattering patterns of Surface#3 (left) and a PEC plate (right) of same size under various polarizations incidences when: (a), (b) ($\theta_{inc} = 30°$, $\varphi_{inc} = 30°$), (c), (d) ($\theta_{inc} = 45°$, $\varphi_{inc} = 45°$), and (e), (f) ($\theta_{inc} = 60°$, $\varphi_{inc} = 60°$).

oblique incidence and its polarization insensitive. When the incident angle is increased and polarization is changed, the 2-D and 3-D scattering patterns of the proposed metasurface have a countless number of low-level lobes in various directions. Furthermore, the proposed metasurface is able to realize wide-angle diffusion for both circularly and LP incidences.

IV. FABRICATION AND MEASUREMENT

To experimentally verify the scattering performance of the proposed metasurface, surface#3 were fabricated using a PCB process. The dielectric substrates is RO4003C and the entire size of the fabricated sample is 160×160 mm^2 and composed of
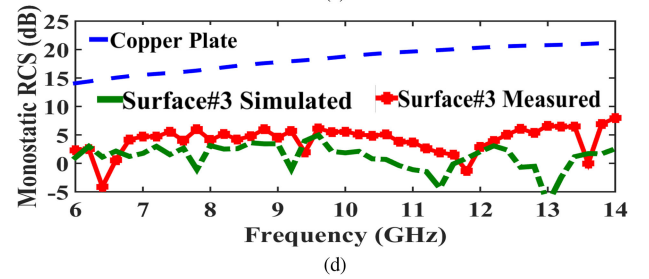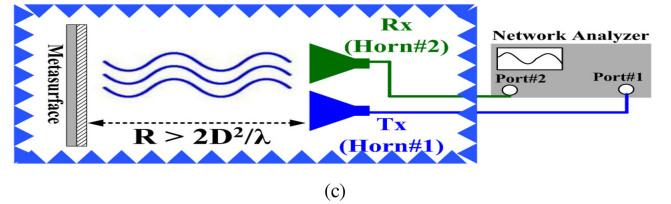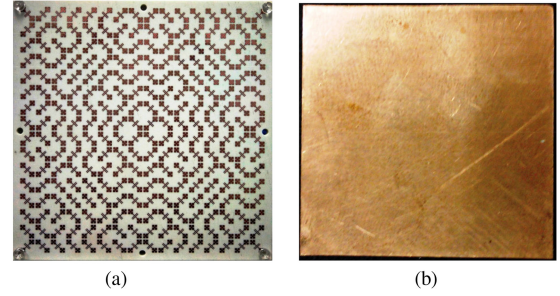

Fig. 9. Photographs of the fabricated samples. (a) Proposed chessboard metasurface (surface#3). (b) Bare copper plate. (c) Measurement setup. (d) Measured RCS.

16×16 unit cells as shown in Fig. 9. The measurement setup inside a microwave chamber is similar to those in the literature [13]–[16] and consists of a two standard gain horn antennas [29] operating from 6 to 14 GHz positioned in front of the surface under test in the far-field region [30] to ensure a plane wave illumination and connected via flexible cables to a vector network analyzer as shown in Fig. 9(c). The transmission coefficient (S_{12}) is used to evaluate the backward scattering. The reflection of a bare copper plate with same size of surface#3 was first measured and used as a reference. The measured monostatic RCS of surface#3 is shown in Fig. 9(d). As can be seen a clear RCS reduction is achieved from 6 to 14 GHz. The little deviation between the measured and simulated results in Fig. 9 can be attributed to the fabrication error, mialignement of the horn antenna, and surface#3 during the measurements.

V. CONCLUSION

In summary, the design of an ultrathin and polarization-independent diffusive modified chessboard like metasurface for low-level diffusion of EM-waves under wide angle of incidence is developed. The four quadrants of a conventional 2×2 chessboard metasurface are replaced by a 1-bit reflectarrays. The 1-bit reflectarrays are designed using a cross-polarization conversion principle with anisotropic unit cell. Both the simulation and measured results are presented.

REFERENCES

[1] H.-X. Xu, "Completely spin-decoupled dual-phase hybrid metasurfaces for arbitrary wavefront control," *ACS Photon.*, vol. 6, no. 1, pp. 211–220, 2018.

[2] T. J. Cui *et al.*, "Information metamaterials and metasurfaces," *J. Mater. Chem. C*, vol. 5, pp. 3644–3688, 2017.

[3] H. X. Xu *et al.*, "Deterministic approach to achieve broadband polarization-independent diffusive scatterings based on metasurfaces," *ACS Photon.*, vol. 5, no. 5, pp. 1691–1702, 2018.

[4] F. Yuan, H. Xu, G. Wang, P. Xie, M. Liu, and K. Wu, "Broadband RCS reduction based on parabolic-phased diffused metasurface," in *Proc. Int. Conf. Microw. Millimeter Wave Technol.*, Chengdu, China, 2018, pp. 1–3.

[5] J. Su, Y. Lu, J. Liu, Y. Yang, Z. Li, and J. Song, "A novel checkerboard metasurface based on optimized multielement phase cancellation for superwideband RCS reduction," *IEEE Trans. Antennas Propag.*, vol. 66, no. 12, pp. 7091–7099, Dec. 2018.

[6] M. Haji-Ahmadi, V. Nayyeri, M. Soleimani, and O. M. Ramahi, "Pixelated checkerboard metasurface for ultra-wideband radar cross section reduction," *Sci. Rep.*, vol. 7, 2017, Art. no. 11437.

[7] H. Xu *et al.*, "Switchable complementary diamond-ring-shaped metasurface for radome application," *IEEE Antennas Wireless Propag. Lett.*, vol. 17, pp. 2494–2497, 2018.

[8] P. Xie, Z. Zhang, Z. Wang, K. Sun, and R. Fan, "Targeted double negative properties in silver/silica random metamaterials by precise control of microstructures," *Research*, vol. 2019, 2019, Art. no. 1021368.

[9] T. Chen, W. Tang, J. Mu, and T. J. Cui, "Microwave metamaterials," *Ann. Phys.*, 2019. [Online]. Available: https://onlinelibrary.wiley.com/doi/10.1002/andp.201800445, Art. no. 1800445.

[10] D. González-Ovejero *et al.*, "Basic properties of checkerboard metasurfaces," *IEEE Antennas Wireless Propag. Lett.*, vol. 14, pp. 406–409, 2015.

[11] C. D. Giovampaola and N. Engheta, "Digital metamaterials," *Nature Mater.*, vol. 13, pp. 1115–1121, 2014.

[12] T. J. Cui, M. Q. Qi, X. Wan, J. Zhao, and Q. Cheng, "Coding metamaterials, digital metamaterials and programmable metamaterials," *Light, Sci. Appl.*, vol. 3, 2014, Art. no. e218.

[13] J. Xue, W. Jiang, and S. Gong, "Chessboard AMC surface based on quasi-fractal structure for wideband RCS reduction," *IEEE Antennas Wireless Propag. Lett.*, vol. 17, pp. 201–204, 2018.

[14] W. Chen, C. A. Balanis, and C. R. Birtcher, "Checkerboard EBG surfaces for wideband radar cross section reduction," *IEEE Trans. Antennas Propag.*, vol. 63, no. 6, pp. 2636–2645, Jun. 2015.

[15] W. Chen, C. A. Balanis, and C. R. Birtcher, "Dual wide-band checkerboard surfaces for radar cross section reduction," *IEEE Trans. Antennas Propag.*, vol. 64, no. 9, pp. 4133–4138, Sep. 2016.

[16] A. Y. Modi *et al.*, "New class of RCS-reduction metasurfaces based on scattering cancellation using array theory," *IEEE Trans. Antennas Propag.*, vol. 67, no. 1, pp. 298–308, Jan. 2019.

[17] A. I. Semenikhin, D. V. Semenikhina, and P. V. Blagovisnyy, "RCS reduction using digital 2-Bit anisotropic impedance metasurfaces," in *Proc. Radiat. Scattering Electromagn. Waves*, 2017, pp. 177–180.

[18] D. Sang, Q. Chen, L. Ding, M. Guo, and Y. Fu, "Design of checkerboard AMC structure for wideband RCS reduction, " *IEEE Trans. Antennas Propag.*, vol. 67, no. 4, pp. 2604–2612, Apr. 2019.

[19] A. Y. Modi, C. A. Balanis, C. R. Birtcher, and H. N. Shaman, "Novel design of ultrabroadband radar cross section reduction surfaces using artificial magnetic conductors," *IEEE Trans. Antennas Propag.*, vol. 65, no. 10, pp. 5406–5417, Oct. 2017.

[20] Y. Han, M. Chen, J. Wang, Z. Zhang, and Z. Li, "Wideband RCS reduction of slot antenna array by using reflectarrays," in *Proc. 6th Int. Symp. IEEE Microw. Antenna, Propag. EMC Technol.*, Shanghai, China, 2015, pp. 201–204.

[21] N. A. Shabayk, H. A. Malhat, and S. H. Zainud-Deen, "Radar cross section reduction using perforated dielectric material and plasma AMC structure," in *Proc. 35th Nat. Radio Sci. Conf.*, Cairo, Egypt, 2018, pp. 47–54,

[22] M. Feng *et al.*, "Two-dimensional coding phase gradient metasurface for RCS reduction," *J. Phys. D, Appl. Phys.*, vol. 51, 2018, Art. no. 372018.

[23] J. Han *et al.*, "Broadband radar cross section reduction using dual-circular polarization diffusion metasurface," *IEEE Antennas Wireless Propag. Lett.*, vol. 17, pp. 969–973, 2018.

[24] H. Luyen, Z. Yang, M. Gao, J. H. Booske, and N. Behdad, "A wideband, single-layer reflectarray exploiting a polarization rotating unit cell," *IEEE Trans. Antennas Propag.*, vol. 67, no. 2, pp. 872–883, Feb. 2019.

[25] S. B. Yeap, X. Qing, and Z. N. Chen, "77-GHz dual-layer transmit-array for automotive radar applications," *IEEE Trans. Antennas Propag.*, vol. 63, no. 6, pp. 2833–2837, Jun. 2015.

[26] A. Massaccesi *et al.*, "3D-printable dielectric transmitarray with enhanced bandwidth at millimeter-waves," *IEEE Access*, vol. 6, pp. 46407–46418, 2018.

[27] M. Akbari, F. Samadi, A. Sebak, and T. A. Denidni, "Super broadband diffuse wave scattering based on coding metasurfaces: polarization conversion metasurfaces," *IEEE Antennas Propag. Mag.*, vol. 61, no. 2, pp. 40–52, Apr. 2019.

[28] S. Sui *et al.*, "Fast optimization method of designing a wideband metasurface without using the pancharatnam–berry phase," *Opt. Express*, vol. 26, no. 2, pp. 1443–1451, 2018.

[29] [Online]. Available: http://www.hdmicrowave.com/index.php.

[30] C. A. Balanis, *Antenna Theory, Analysis and Design*, 2nd ed. New York, NY, USA: Wiley, 1996.